Electronic properties and photoelectron circular dichroism of adsorbed chiral molecules

L. Ferrari,[1,*] P. Moras,[2] P. Gori,[3,†] S. Turchini,[3] N. Zema,[3] A. Palma,[4] J. Fujii,[5] I. Vobornik,[5] G. Alejandro,[6] D. Catone,[3] T. Prosperi,[3] and C. Carbone[2]

[1]*Istituto dei Sistemi Complessi, Consiglio Nazionale delle Ricerche, Roma I-00133, Italy*
[2]*Istituto di Struttura della Materia, Consiglio Nazionale delle Ricerche, Trieste I-34149, Italy*
[3]*Istituto di Struttura della Materia, Consiglio Nazionale delle Ricerche, Roma I- 00133, Italy*
[4]*Istituto per lo Studio dei Materiali Nanostrutturati, Consiglio Nazionale delle Ricerche, Montelibretti I-00015, Italy*
[5]*Istituto Officina dei Materiali, TASC Laboratory, Consiglio Nazionale delle Ricerche, Trieste I-34014, Italy*
[6]*International Center for Theoretical Physics (ICTP), Trieste I-34014, Italy*

(Received 3 October 2014; revised manuscript received 22 December 2014; published 6 February 2015)

We report on an angle-resolved photoemission investigation of the valence states and chiral properties of a nonchirally oriented phase of tartaric acid deposited on a Cu(110) surface, observed with circularly polarized light. The two optical enantiomers R,R and S,S of tartaric acid, separately deposited, produce (40,23) overlayers which show a large dichroic effect and enantiomeric behavior all over the valence energies. The dichroic effects are displayed by native chiral molecular states and molecule-copper interface states. Density-functional theory calculations of the site-resolved density of states analyze the formation of hybrid states at the tartaric acid-copper interface and suggest that an observed interface state acquires chirality on binding.

DOI: 10.1103/PhysRevB.91.085408 PACS number(s): 79.60.−i, 33.55.+b, 71.15.−m

I. INTRODUCTION

Chiral molecules adsorbed on surfaces, ordered with local or long-range chirality, are interesting for molecular recognition in the fields of heterogeneous catalysis and selective chemical reactivity [1–4]. Metal surfaces, covered with specific chiral molecules, are used to induce the preferential synthesis of particular enantiomers. The identification and control of the chiral nature of adsorbed molecules is an important research target, though generally not easily achievable. Angle-resolved photoemission spectroscopy (ARPES) can provide a picture of the chiral properties of adsorbates on surfaces when circularly polarized radiation is used. Theoretical [5–7] and experimental [8–10] studies of circular dichroism in the photoemission of spatially oriented chiral molecules on metal and semiconductor surfaces show an asymmetric effect in the angular distribution of the photoelectrons emitted from core levels and valence states. Circular dichroism in the angular distribution (CDAD) of the photoelectrons is described in a pure electric dipole approximation, and the amplitude of the asymmetry effect is expected to be of the same order of the differential cross section for left and right circularly polarized light [5]. The observed asymmetry from a C 1*s* core level of alanine on Cu(110), for instance, reaches a maximum of about 5% in the chiral center of the molecule. [9] CDAD effects, directly observable in photoemission from molecular valence states, can be larger, as will be shown in this paper.

Tartaric acid (TA) is one of the most studied chiral modifiers of crystalline metal surfaces. When TA is deposited on surfaces, it arranges in various ordered adsorption phases depending on the temperature and coverage conditions, adopting a monotartrate or bitartrate form, with local or global chirality, as already extensively studied with scanning tunneling microscopy (STM) and infrared spectroscopy [11,12]. In this paper we investigate the valence states of the ordered (40,23) superstructures formed by pure R,R or S,S enantiomers of TA assembled on Cu(110) by means of angle-resolved photoemission spectroscopy using circularly polarized light. Density-functional theory (DFT) calculations were performed to derive a model of the adsorption geometry and to determine the corresponding electronic properties. The (40,23) superstructure is achiral [13], which, due to the absence of global chiral behavior, is perfectly superimposable on its mirror image. Nonglobally chiral overlayers of pure enantiomers thus offer the possibility to study the manifestation of chirality at the local level without interference from additional chiral effects [14,15]. We report the observation of strong CDAD effects in the valence state emission from TA superstructures. In particular, we address the bonding effects between the molecules and substrate and discuss how the chiral character of the deposited molecules can be transferred to a nonchiral surface, through the formation of interface states.

II. EXPERIMENTAL AND THEORETICAL DETAILS

The (40,23) self-assembled molecular structure was obtained *in situ* following the well-established procedure [1,16] of the sublimation of a pure R,R (S,S) enantiomer of TA on a clean Cu(110) substrate, prepared by cycles of 500 eV Ar ion sputtering and annealing at 700 K. TA was deposited on the crystal at 300 K.

Photoemission measurements of the valence states and their k-resolved maps were performed at room temperature using a Scienta SES 2002 analyzer of the APE beamline at the Elettra synchrotron radiation facility, with circularly polarized radiation at a photon energy of 25 eV. Dichroic effects were examined by comparing photoemission spectra obtained with circularly polarized light of opposite helicity, through multichannel acquisition and angular scans with in-plane geometry and an angular resolution of better than 0.2°. The degree of circular polarization of the photon beam

*Corresponding author: luisa.ferrari@isc.cnr.it
†Present address: Dipartimento di Ingegneria, Università Roma Tre, Roma I-00146, Italy.

 ©2015 American Physical Society

on the sample is estimated to be 90% at the photon energy used, for right and left polarization. Enantiomer-dependent CDAD effects were observed upon switching the light helicity. In general, this effect on surfaces might be overpowered by the geometry of the experiment, which can yield additional dichroic effects even in the case of nonchiral systems, unless the plane of the incident light and the photoelectron collection direction correspond to a mirror symmetry plane of the substrate [17,18]. In our experiment the incident light direction formed an angle of 45° with the analyzer axis. The sample was measured along the $\bar{\Gamma}$-$\bar{Y}$ direction of the substrate. The surface normal, the incident light, and the photoelectron directions are coplanar in the $\bar{\Gamma}$-$\bar{Y}$ mirror plane of the Cu substrate. A sketch of the experimental geometry is included in Fig. 3. Supplementary data were acquired at the VUV-Photoemission beamline (Elettra).

DFT calculations were performed using the plane-wave pseudopotential code QUANTUM ESPRESSO [19]. The employed pseudopotentials make use of a semilocal generalized gradient approximation with a Perdew-Burke-Ernzerhof (GGA-PBE) treatment of exchange and correlation energy [20,21]. A kinetic energy cutoff of 25 Ry was used in the plane-wave expansion. The system was represented in a repeated slab approach, with a (40,23) surface cell to describe the corresponding adsorption phase. The Cu(110) surface was modeled by a seven-layer slab separated by 21.2 Å of vacuum from its periodic replicas along the direction perpendicular to the surface. The surface Brillouin zone was sampled by a 4×3 Monkhorst-Pack mesh of k points [22]. The system was relaxed using the Broyden-Fletcher-Goldfarb-Shanno algorithm [23–26] until the forces on each ion were reduced below 10^{-4} a.u. and the crystal cell parameters were kept fixed. The approximate exchange-correlation density functional used is capable of good accuracy in the description of chemical bonds, but it is not expected to properly describe weak physical interactions, such as van der Waals ones or noncovalent bonds. To overcome this limitation we evaluated the dispersion forces [27,28] by means of a semiempirical GGA-type density functional constructed with a long-range correction. The total energy of the system is obtained by adding the semiempirical dispersion contribution to the self-consistent Kohn-Sham energy [29,30].

III. RESULTS AND DISCUSSION

The TA molecule (HOOC-CHOH-CHOH-COOH) has two carboxylic groups (COOH) potentially involved in bonding to the surface and two chiral centers along the backbone of the molecule. In the (40,23) structure a close packed aggregate of monotartrate (the singly deprotonated form of TA) forms a full monolayer. A model with two anchorage points was suggested based on STM images [1] and on a recent quantitative structural model based on scanned-energy mode photoelectron diffraction experiments [31]. We determined the most stable R,R-TA conformer in the (40,23) phase by means of DFT calculations and modeled its configuration on Cu(110) to obtain an accurate description of the electronic properties of the system. We studied the relative stability of several R,R-TA conformers in the (40,23) phase, both with two and three anchorage points. We found that a geometry with three

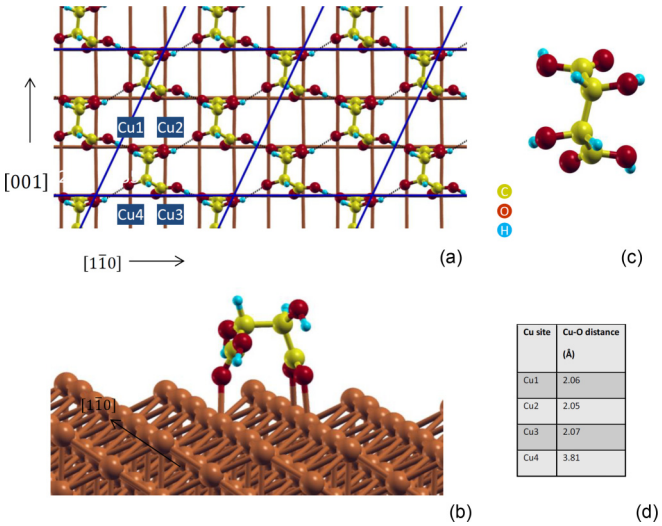

FIG. 1. (Color online) (a), (b) Most stable adsorption geometry for TA/Cu(110) in the (40,23) phase. The copper atoms $Cu_{1,2,3,4}$ are located in the intersection points of the grid. The dashed black lines highlight intermolecular bonds. (c) Most stable R,R-TA conformer in the (40,23) superstructure. (d) Theoretical values of the distances between the oxygen and copper atoms in the adsorption sites as labeled in (a).

anchorage points is more stable, by 0.68 eV/molecule, than the most stable conformer with two anchorage points. The optimized adsorption geometry for the (40,23) superstructure is reported in Figs. 1(a) and 1(b), together with a top view of the most stable R,R-TA conformer for this surface superstructure [Fig. 1(c)]. The unit cell of the (40,23) superstructure includes three molecules of monotartrate. According to DFT results, a bridge bonded bidentate at one end and a monodentate at the other end of the TA molecule is formed on the Cu(110) surface. Each molecule is then bonded to three different surface Cu atoms, labeled in Fig. 1(a) as Cu_1, Cu_2, and Cu_3, through two oxygen atoms of the deprotonated carboxylate group (O_1, O_2 at one end of the molecule) and one oxygen of the other carboxyl group not deprotonated (O_5 at the other end of the molecule), respectively. In this configuration the three carboxylic oxygen atoms sit on top of three copper atoms at distances of 2.06, 2.05, and 2.07 Å, respectively. The interatomic distances determined in our work are in the range of standard copper-oxygen metal complexes [32]. The metal-molecule interaction takes place through the carboxylic groups which point toward the surface while the hydroxyl groups lie almost parallel to the surface and have the role of establishing the hydrogen bond network within the self-assembled structure. This local geometry partly resembles the configuration with three anchorage points for each TA molecule that has been recently found by DFT [33], which, however, refers to a transition state in the bitartrate formation and to a different surface superstructure.

The low-energy electron diffraction (LEED) pattern of the R,R-TA enantiomer forming the (40,23) superstructure is shown in Fig. 2. The same result is obtained for the S,S-TA enantiomer. The LEED pattern preserves reflection symmetry with respect to the (001) and (1$\bar{1}$0) planes of the Cu(110) substrate, indicating that the system does not have a global

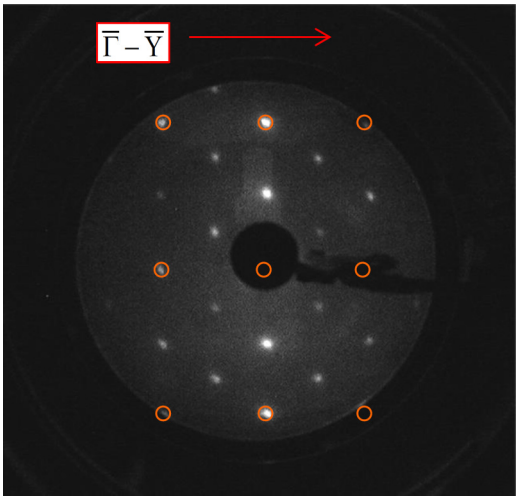

FIG. 2. (Color online) LEED pattern from the TA/Cu(110) (40,23) phase. Red circles enclose the (1 × 1) spots of the Cu(110) surface.

surface chirality. ARPES data acquired with the two light helicities for R,R-TA molecules on Cu(110) in the (40,23) phase along the $\bar{\Gamma}$-$\bar{Y}$ direction are shown in Fig. 3(a). The dichroic effect in the photoemission spectra is up to 20% for specific binding energies and emission angles. Corresponding spectra were recorded for the S,S-TA enantiomer in the same experimental condition. Several spectral features observed in the photoemission spectra show circular dichroism. Color maps representing the CDAD in the photoemission signal for the two enantiomers are shown in Fig. 3(b). The data report the difference between the photoemission intensity acquired with right circularly polarized (RCP) and left circularly polarized (LCP) light, normalized by their sum in order to remove the cross-section dependence: $(I_{\mathrm{RCP}} - I_{\mathrm{LCP}})/(I_{\mathrm{RCP}} + I_{\mathrm{LCP}})$. This value is calculated after the subtraction of an integral background curve from each spectrum. The results in Fig. 3(b) show that the CDAD signal displays an almost full sign reversal upon changing the enantiomer. The maps thus demonstrate that the observed dichroic effect largely arises from the local molecular chirality rather than from the experimental geometry.

In Fig. 4(a) we compare experimental spectra and the theoretical density of states (DOS) for the TA/Cu(110) system, and the photoemission spectra of the free TA molecule in the gas phase and the bare Cu surface. The valence band structure measured from −14 to −4.5 eV below the Fermi level mostly reflects the almost pure molecular states originating from s and p atomic orbitals. The structures at higher binding energies (−9.4 and −12.8 eV) were used to align the photoemission spectra for the molecules in the gas phase and for the deposited TA. These states are assigned on the basis of our DFT calculations to the s and p molecular states of carbon and alcoholic oxygen atoms not strongly perturbed by the surface interaction. The comparison between theoretical calculations and experimental data [in Fig. 4(a)] shows a good agreement, taking account of the arbitrary broadening used in the calculations and the experimental resolution.

The energy range between −4 and 0 eV below the Fermi level, where the relatively narrow Cu d band gives rise to

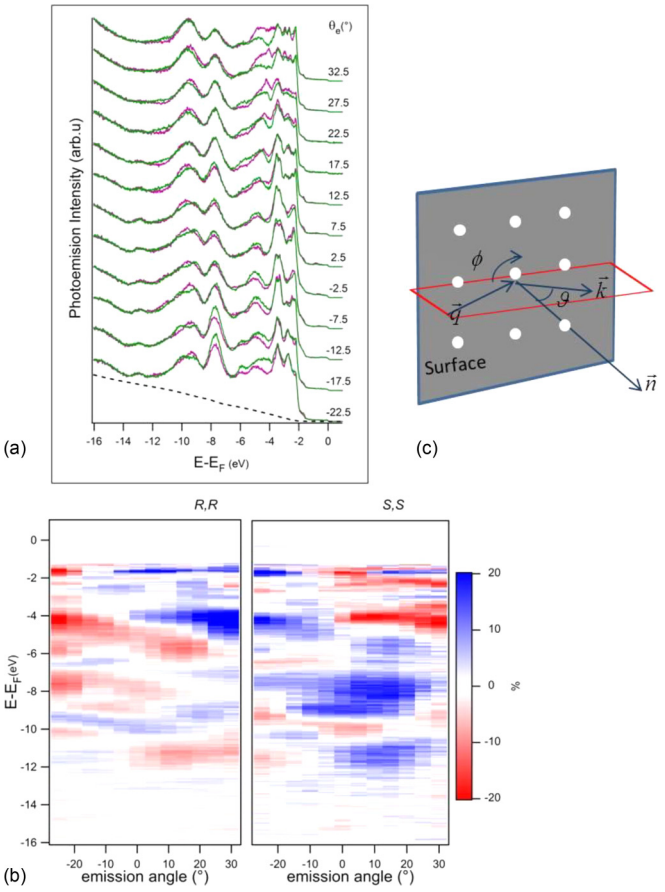

FIG. 3. (Color online) (a) Valence band photoemission spectra of a R,R enantiomer of TA molecules on Cu(110) in the (40,23) phase, taken at different emission angles with circularly polarized light of 25 eV of photon energy. In magenta, the spectra acquired with right-handed helicity of incident radiation, in green those acquired with left-handed helicity, and the dashed line is the integral background curve subtracted to each photoemission spectrum. (b) Maps of the dichroic signal, for the two enantiomers R,R and S,S acquired with circularly polarized light. (c) Sketch of the experimental geometry.

a strong interaction predominantly with p states of the carboxylic oxygen atoms, is instead of interest for understanding the molecule-substrate coupling. The comparison between the valence band spectra of Cu(110) before and after TA deposition indicates the appearance, in the latter case, of a shoulder near 1.7 eV of binding energy on the onset of the d band and other states superimposed on the Cu d band. The comparison between the gas phase and TA/Cu experimental spectra indicates that the feature at 1.7 eV binding energy should be not related to the highest occupied molecular orbital (HOMO) of the monotartrate molecule. To analyze such an interaction we calculated the projected density of states (PDOS) for the TA/Cu(110) system. In Fig. 4(b) we report the PDOS at the $\bar{\Gamma}$ point for the p orbitals of the interacting (O_1, O_2, and O_5) and noninteracting (O_4) carboxylic oxygen atoms, the PDOS of the d orbitals for a copper atom strongly interacting with TA [Cu_1 in Fig. 1(a)], and that of a bare surface copper. The calculations suggest that the peak located at −1.25 eV arises from the molecule-surface interaction. This

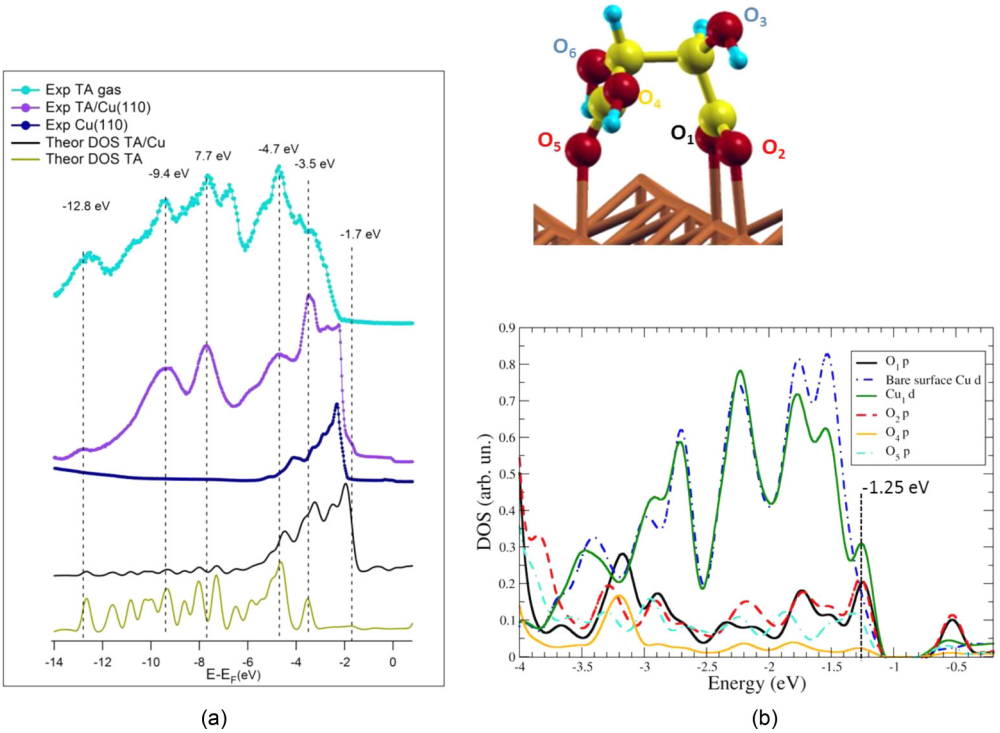

FIG. 4. (Color online) (a) Comparison between the experimental photoemission data for TA molecules in the gas phase and TA/Cu system, calculated DOS for the TA/Cu system, and the difference (in olive green) between TA/Cu system DOS and Cu DOS. (b) DFT PDOS on selected TA/Cu(110) atoms. Labeling is explained in the top part of the figure. Oxygen PDOS have been multiplied by a factor 8 for better visualization.

feature can be associated with the experimental peak observed at −1.7 eV, considering that DFT is known to produce a down shift of 0.3−0.5 eV for Cu 3*d* states with respect to the experiment [34]. Furthermore, we can identify the structures in the O_1, O_2, and O_5 PDOS resulting from the interaction with the Cu(110) surface, which are absent in the PDOS of O_4.

The molecule-metal interaction manifests itself through orbital hybridization with the formation of bonding states overimposed on the Cu *d* bands and antibonding states at the onset of Cu *d* bands, as the Anderson-Newns model predicts [35]. Theoretical calculations [36] and experimental observations [10] have recently shown this picture to apply for organic molecules on Cu(110). Our calculations ascribe the theoretical features at −1.25 and −1.74 eV to antibonding states and those at −2.90, −3.17, and −3.27 eV to bonding states [Fig. 4(b)]. They arise from the hybridization between the 2*p* states of the carboxylic oxygen and the 3*d* Cu states, with a prevalence of d_{z^2} character for the antibonding and d_{xy} for the bonding states. The nature of these hybrid states is clarified by the squared wave functions of the (40,23) TA/Cu(110) system corresponding to the peaks in the carboxylic oxygen PDOS (O_1, O_2, and O_5). In Fig. 5 we show the charge distribution calculated at the $\bar{\Gamma}$ point for the theoretical eigenvalues −2.90 eV [Fig. 5(a)] and −1.25 eV [Fig. 5(b)]. The bonding state has charge distributed along the direction connecting the Cu and O atoms [Fig. 5(a)], while the charge is localized around the two atoms for the antibonding state [Fig. 5(b)].

With the further support of this result, we associate the experimentally observed feature at −1.7 eV to the antibonding state at −1.25 eV. Conversely, the experimental identification of the bonding states is difficult, due to the overlap with the Cu *d* band. In addition, the adsorption of ordered layers of organic molecules on noble metal surfaces can affect the photoemission line shape of the *d* bands and makes a simple analysis unreliable [37].

The CDAD properties of the antibonding state at −1.7 eV are further illustrated in Fig. 6. As an example, Fig. 6(a)

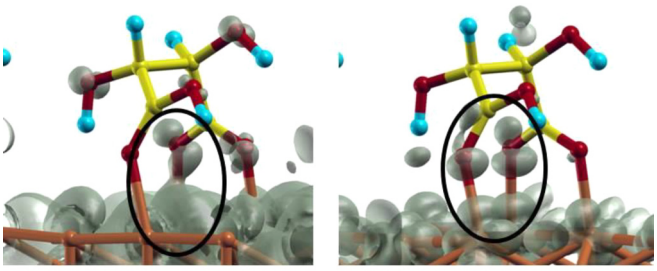

FIG. 5. (Color online) The gray regions represent the squared wave functions for the TA/Cu(110) system calculated at the $\bar{\Gamma}$ point for the theoretical eigenvalues (a) −2.90 and (b) −1.25 eV. In orange, the Cu atoms in the ball-and-stick representation as well as the TA atoms represented in yellow (carbon atoms), red (oxygen), and cyan (hydrogen).The isodensity levels are (a) 5.4×10^{-5} $e/(\text{Å}^3)$ and (b) 8.1×10^{-4} $e/(\text{Å}^3)$.

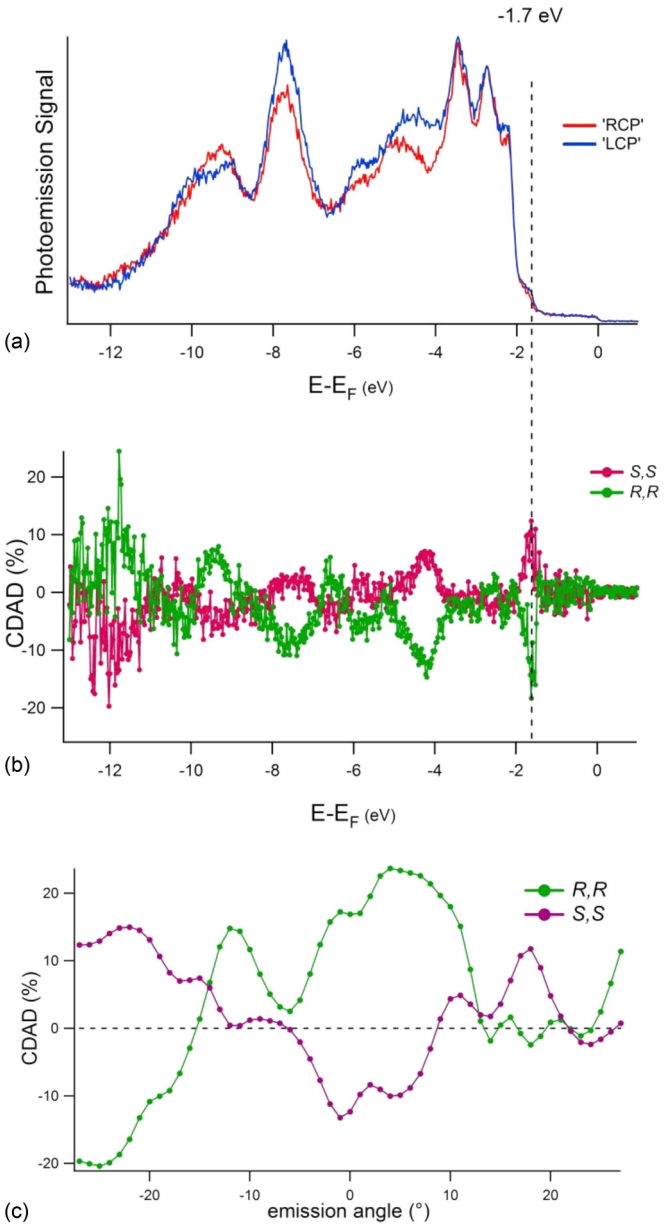

FIG. 6. (Color online) (a) RCP and LCP photemission spectra of a R,R-TA enantiomer in the (40,23) adsorbed phase at -21° off normal emission. (b) Corresponding CDAD signal for the two R,R- and S,S-TA enantiomers. (c) CDAD signal obtained for the feature at -1.7 eV as a function of the emission angle.

shows RCP and LCP photoemission spectra of the R,R-TA enantiomer at the $\bar{Y}$ point of the surface Brillouin zone of Cu(110). The corresponding dichroic spectrum, along with that for the S,S enantiomer, is reported in Fig. 6(b). When the intensity of the dichroic signal at -1.7 eV is plotted as a function of the emission angle [Fig. 6(c)], the enantiomer-specific behavior of this feature becomes clear. The observed asymmetry can be attributed to an effect resulting from the initial or final state chirality, or from their combination. It is known that CDAD can arise from the dissymmetry of the final state wave function in the dipole matrix element, also in the absence of ground state chirality [38]. On the other side, the antibonding character of the orbital shown by the computations in Fig. 5(b) demonstrates that its nature is that of a metal-molecule hybrid state with a charge distribution reflecting the geometry of the enantiomer. This suggests that the observed CDAD can be associated with the chirality of the initial states and that a chiral character is transferred to the interface.

IV. CONCLUSIONS

We studied the electronic structure of TA chiral molecules arranged on the Cu(110) surface in the (40,23) phase by ARPES and focused on their dichroic behavior using circularly polarized radiation. We presented a model of the adsorption geometry and combined the observations of CDAD effects with DFT calculations. We showed that the CDAD effects are large for the molecular states and that the adsorption process gives rise to hybrid interface states. The strong CDAD signal of the interface state at -1.7 eV in the valence band photoemission spectrum can be attributed to the local chiral electronic interaction between TA and the bonded Cu atom underneath the molecule, providing a spectroscopic indication of chirality transfer. The CDAD effect helps to interpret the electronic structure, to disentangle chiral states, and can find application in the analysis of organic molecules on metal surfaces and surface chirality in general.

ACKNOWLEDGMENTS

We would like to thank Dr. M. Satta for the preliminary calculations of TA conformers in the gas phase. CPU time has been granted by Enea-Cresco.

[1] S. M. Barlow and R. Raval, Surf. Sci. Rep. **50**, 201 (2003).
[2] A. Kuehnle, T. R. Linderoth, B. Hammer, and F. Besenbacher, Nature (London) **415**, 891 (2002).
[3] R. Raval, J. Mol. Catal. A: Chem. **305**, 112 (2009).
[4] Y. Izumi, M. Imaida, H. Fukawa, and S. Akabori, Bull. Chem. Soc. Jpn. **36**, 21 (1963).
[5] N. A. Cherepkov, Chem. Phys. Lett. **87**, 344 (1982).
[6] B. Ritchie, Phys. Rev. A **12**, 567 (1975).
[7] N. Chandra, Phys. Rev. A **39**, 2256 (1989).
[8] J. W. Kim, M. Carbone, J. H. Dil, M. Tallarida, R. Flammini, M. P. Casaletto, K. Horn, and M. N. Piancastelli, Phys. Rev. Lett. **95**, 107601 (2005).
[9] M. Polcik, F. Allegretti, D. I. Sayago, G. Nisbet, C. L. A. Lamont, and D. P. Woodruff, Phys. Rev. Lett. **92**, 236103 (2004).
[10] G. Contini, S. Turchini, S. Sanna, D. Catone, J. Fujii, I. Vobornik, T. Prosperi, and N. Zema, Phys. Rev. B **86**, 035426 (2012).
[11] V. Humblot and R. Raval, App. Surf. Sci. **241**, 150 (2005).
[12] M. Ortega Lorenzo, C. J. Baddeley, C. Muryn, and R. Raval, Nature (London) **404**, 376 (2000).
[13] M. Ortega Lorenzo, S. Haq, P. Murray, R. Raval, and C. J. Baddeley, J. Chem. B **103**, 10661 (1999).
[14] J. Seifert, M. Busch, E. Meyer, and H. Winter, Phys. Rev. B **89**, 075404 (2014).

[15] J. Seifert, M. Busch, E. Meyer, and H. Winter, Phys. Rev. Lett. **111**, 137601 (2013).
[16] T. J. Lawton, V. Pushkarev, D. Wei, F. R. Lucci, D. S. Sholl, A. J. Gellman, and E. H. Sykes, J. Phys. Chem. C **117**, 22290 (2013).
[17] F. Allegretti, M. Polcik, D. I. Sayago, F. Demirors, S. O'Brien, G. Nisbet, C. L. A. Lamont, and D. P. Woodruff, New J. Phys. **7**, 109 (2005).
[18] C. Westphal, J. Bansmann, M. Getzlaff, and G. Schönhense, Phys. Rev. Lett. **63**, 151 (1989).
[19] P. Giannozzi *et al.*, J. Phys.: Condens. Matter **21**, 395502 (2009).
[20] J. P. Perdew, K. Burke, and M. Ernzerhof, Phys. Rev. Lett. **77**, 3865 (1996).
[21] J. P. Perdew, K. Burke, and M. Ernzerhof, Phys. Rev. Lett. **78**, 1396 (1997).
[22] H. J. Monkhorst and J. D. Pack, Phys. Rev. B **13**, 5188 (1976).
[23] C. G. Broyden, J. Inst. Math. Appl. **6**, 76 (1970).
[24] R. Fletcher, Comput. J. **13**, 317 (1970).
[25] D. Goldfarb, Math. Comput. **24**, 23 (1970).
[26] D. F. Shanno, Math. Comput. **24**, 647 (1970).
[27] S. Grimme, J. Comput. Chem. **25**, 1463 (2004).
[28] S. Grimme, J. Comput. Chem. **27**, 1787 (2006).
[29] C. Zazza, N. Sanna, and A. Palma, J. Phys. Chem. A **113**, 14813 (2009).
[30] G. Contini *et al.*, Langmuir **27**, 7410 (2011).
[31] D. A. Duncan, W. Unterberger, D. C. Jackson, M. K. Knight, E. A. Kroger, K. A. Hogan, C. L. A. Lamont, T. J. Lerotholi, and D. P. Woodruff, Surf. Sci. **606**, 1435 (2012).
[32] M. Melnik, Coord. Chem. Rev. **36**, 1 (1981).
[33] J. Zhang, T. Lu, C. Jiang, J. Zou, F. Cao, and Y. Chen, J. Chem. Phys. **131**, 144703 (2009).
[34] V. N. Strocov, R. Claessen, F. Aryasetiawan, P. Blaha, and P. O. Nilsson, Phys. Rev. B **66**, 195104 (2002).
[35] B. Hammer and J. K. Nørskov, Adv. Catal. **45**, 71 (2000).
[36] N. Atodiresei, K. Schroeder, and S. Blügel, Phys. Rev. B **75**, 115407 (2007).
[37] L. Giovanelli *et al.*, Phys. Rev. B **87**, 035413 (2013).
[38] J. Bansmann, Ch. Ostertag, G. Schönhense, F. Fegel, C. Westphal, M. Getzlaff, F. Schafers, and H. Petersen, Phys. Rev. B **46**, 13496 (1992).